Pergamon

Int. J. Solids Structures Vol. 31, No. 14, pp. 1923–1948, 1994

0020–7683/94 $7.00 + .00

0020–7683(93)E0024–C

EFFECT OF TRANSFORMATION-INDUCED SHEAR STRAINS ON CRACK GROWTH IN ZIRCONIA-CONTAINING CERAMICS

G. TH. M. STAM, E. VAN DER GIESSEN and P. MEIJERS
Laboratory for Engineering Mechanics, Faculty of Mechanical Engineering and Marine Technology, Delft University of Technology, Delft, The Netherlands

(*Received* 24 *January* 1993; *in revised form* 3 *November* 1993)

Abstract—Finite element analysis is used to study the crack growth behaviour of ceramics containing tetragonal zirconia, which can undergo a stress-induced martensitic transformation with both dilatation and shear strain components. The finite element model is based on a continuum theory which describes the plastic, pseudo-elastic and shape memory behaviour of such ceramics due to the phase transition. First, the continuum model is used to study the possibility of strain localization phenomena, and the associated loss of ellipticity of the governing equations is taken as an indicator of critical transformations. Based on these results a set of parameters is generated which guarantee subcritical transformation behaviour. Next, mode I crack growth simulations are performed by using an incremental loading algorithm with a nodal release technique to simulate crack advance when the critical stress intensity at the crack tip is reached. The development of the transformation zone near the crack tip is studied in detail, focusing in particular on the effect of the transformation shear component. Transformation zones and crack growth resistance curves are given to make comparison with experiments feasible. It is found that the shear component of the transformation, which has been neglected in most previous investigations, has an important influence on the toughening behaviour.

1. INTRODUCTION

It is well known that the fracture toughness of zirconia (ZrO_2)-containing ceramics can be greatly enhanced by the stress-induced martensitic-type transformation in zirconia particles (Evans and Heuer, 1980; Green *et al.*, 1989). This toughening mechanism has been applied in, for instance, partially stabilized zirconia (PSZ), tetragonal zirconia polycrystal (TZP) and zirconia toughened alumina (ZTA) materials. In an unconstrained zirconia particle, this transformation from the tetragonal structure to the monoclinic structure, $t \rightarrow m$, is accompanied by a volume expansion of about 4.5% and a shear strain of about 16%. However, the resulting shear strains in a constrained particle are much less, since twinning occurs where the sense of the different shear bands alternates from one band to the next.

The early, pioneering constitutive model developed by McMeeking and Evans (1982), and by Budiansky *et al.* (1983) completely neglected the transformation-induced shear strains associated with the $t \rightarrow m$ transformation as these shear strains were assumed to remain small because of twinning. This so-called "dilatant transformation" model has significantly enlarged the understanding of transformation toughening, but there is unsatisfactory quantitative agreement with experiments [see, for example, Evans and Cannon (1986)]. Work of Lambropoulos (1986) has revealed that the influence of the transformation shear component on the shape of the transformation zone may be quite substantial. By means of an approximate analysis, he determined a toughening effect which is in better agreement with experiments. In Lambropoulos' continuum model, twinning is assumed to relax all shear stresses in the transforming particle, while he further assumes that the phase transition in all particles occurs instantaneously and completely. Furthermore, his analysis neglects the coupling between transformation and the disturbance of the crack tip fields due to transformation. Despite the very approximate nature of this analysis, Lambropoulos' (1986) conclusions have certainly triggered further research into the effect of transformation-induced shear strains (Stump, 1991; Budiansky and Truskinovsky, 1993).

Recently, increasing experimental evidence has been found for the occurrence of significant transformations shear strains. For instance, Chen and Reyes-Morel (1986, 1987) and Reyes-Morel and Chen (1988) presented results of hydraulic compression experiments which showed shear and dilatation effects of comparable magnitude. Based on these and related observations, Sun *et al.* (1991) developed a new, micromechanics-based continuum model to account for both the dilatant and shear transformation effects. Here, we adopt this model, and use it to study the influence on the shape and size of the transformation zone as well as on the toughening during crack growth.

The paper is organized as follows. First, a brief introduction to the constitutive model is given, followed by a stability analysis of the governing equations in Section 3. In particular, the deformation response during transformation is studied to detect conditions under which localization may occur due to the loss of ellipticity of the equations. The possibility of loss of ellipticity has also been observed in the purely dilatant model, where Budiansky *et al.* (1983) termed the corresponding transformation behaviour "supercritical". From the stability analysis, the governing parameters for localization to occur in the presence of transformation-induced shear strains are found, together with their critical combination.

In Section 4 the crack growth problem is formulated, followed by the presentation of the numerical method that is used to solve the problem. Transient crack growth is simulated in a finite element model by a nodal release technique. A parameter study has been carried out to explore the influence of the strength of the transformation, the transformation hardening and, in particular, the contribution of transformation shear strains on the transformation behaviour and on the crack growth development. The results of a number of detailed computations are presented in Section 6 in terms of predicted transformation zones and crack growth resistance curves. The results according to the adopted constitutive model show that the shear transformation strains have a very significant influence on both the transformation zone and the toughness increase.

Standard tensor notation is used, with tensors being denoted with bold-face characters. Cartesian components with indices running from 1 to 3 are indicated with Latin subscripts, while Greek subscripts run from 1 to 2 only. The second-order unit tensor is $\mathbf{I}$, and tr denotes the trace. The tensor produce is denoted by $\otimes$ and the following operations apply to any fourth-order tensor $\mathbf{L}$ and second-order tensors $\mathbf{A}$ and $\mathbf{B}$: $\mathbf{LA} = L_{ijkl}A_{kl}(\mathbf{e}_i \otimes \mathbf{e}_j)$, $\mathbf{A}\cdot\mathbf{B} = A_{ij}B_{ij}$. A superposed dot denotes the time derivative; but since we will not be concerned with true time-dependent phenomena, any monotonically increasing parameter may serve as "time" parameter.

2. CONSTITUTIVE BEHAVIOUR

In this section we first summarize the constitutive relations proposed by Sun *et al.* (1991) followed by a brief comparison of the model to experimentally derived stress–strain curves. Finally we show the relation of this model to the dilatant transformation model.

Constitutive equations

In this paper we use the constitutive equations proposed by Sun *et al.* (1991) to model the inelastic behaviour of an isotropic composite material that is assumed to consist of a linear elastic isotropic matrix (referred to with the index M) containing linear elastic isotropic inclusions (referred to with the index I). These inclusions are metastable tetragonal particles, which can undergo (eventual reversible) phase transformation involving shear and dilatation effects. It is assumed that a small representative material sample (constitutive element) can be taken such that the transformation zone contains a large number of these constitutive elements, so that a continuum description of the composite can be formulated. Hence, the constitutive element is assumed to consist of a large number of transformable inclusions. These quantities in the inside of the constitutive element are considered to be microscopic quantities and are denoted with lower-case characters. Macroscopic quantities are referred to with upper-case characters, and can be found by taking the volume average $\langle\cdot\rangle$ of the microscopic quantities of the constitutive element. For instance, the microscopic stress and strain tensors are indicated by $\boldsymbol{\sigma}$ and $\boldsymbol{\varepsilon}$, respectively, and with a given volume

fraction of second phase (transformable metastable tetragonal inclusions) f^m, the relation between microscopic and macroscopic stresses is

$$\boldsymbol{\Sigma} = \langle \boldsymbol{\sigma} \rangle_V = \frac{1}{V} \int_V \boldsymbol{\sigma} \, \mathrm{d}V = f^m \langle \boldsymbol{\sigma} \rangle_{V_I} + (1 - f^m) \langle \boldsymbol{\sigma} \rangle_{V_M}, \tag{1}$$

where the volumes of the element, matrix and inclusions are given by V, V_M and V_I, respectively.

The strains are assumed to be small and, assuming isothermal deformations, can be decomposed into an elastic part $\mathbf{E}^e$ and a "plastic" part $\mathbf{E}^p$ due to the $t \to m$ transformation in the inclusions, which is given by

$$\mathbf{E}^p = f \langle \boldsymbol{\varepsilon}^p \rangle_{V_I}, \tag{2}$$

where f is the actual fraction of transformed volume which is obviously smaller than or equal to f^m. The $t \to m$ phase transition involves dilatational and shear strains within the inclusion, thus suggesting to split the plastic strain into a dilatational part and a deviatoric part, designated with superscripts d and s, respectively

$$\mathbf{E}^p = \mathbf{E}^{pd} + \mathbf{E}^{ps} = f \langle \boldsymbol{\varepsilon}^{pd} \rangle_{V_I} + f \langle \boldsymbol{\varepsilon}^{ps} \rangle_{V_I}. \tag{3}$$

The rates of plastic strain during progressive transformation ($\dot{f} > 0$) can be obtained by straightforward differentiation of (3), but also from the average of the transformation strain $\boldsymbol{\varepsilon}^p$ over the freshly transformed inclusions, i.e.

$$\begin{aligned} \dot{\mathbf{E}}^p = \dot{\mathbf{E}}^{pd} + \dot{\mathbf{E}}^{ps} &= \dot{f} \langle \boldsymbol{\varepsilon}^{pd} \rangle_{V_I} + \dot{f} \langle \boldsymbol{\varepsilon}^{ps} \rangle_{V_I} + f \overline{\dot{\langle \boldsymbol{\varepsilon}^{pd} \rangle}_{V_I}} + f \overline{\dot{\langle \boldsymbol{\varepsilon}^{ps} \rangle}_{V_I}} \\ &= \dot{f} \langle \boldsymbol{\varepsilon}^{pd} \rangle_{\mathrm{d}V_I} + \dot{f} \langle \boldsymbol{\varepsilon}^{ps} \rangle_{\mathrm{d}V_I}. \end{aligned} \tag{4}$$

The dilatational part $\boldsymbol{\varepsilon}^{pd}$ within each inclusion is given by $\boldsymbol{\varepsilon}^{pd} = (\frac{1}{3} \operatorname{tr} \boldsymbol{\varepsilon}^{pd}) \mathbf{I} = \varepsilon^{pd} \mathbf{I}$ in terms of the constant stress-free lattice dilatation ε^{pd} which typically takes a value of 1.5% at room temperature; hence

$$\langle \boldsymbol{\varepsilon}^{pd} \rangle_{\mathrm{d}V_I} = \langle \boldsymbol{\varepsilon}^{pd} \rangle_{V_I} \equiv \boldsymbol{\varepsilon}^{pd} = \varepsilon^{pd} \mathbf{I}. \tag{5}$$

The average deviatoric part $\mathbf{E}^{ps}$ is significantly less than the stress-free lattice shear strain of 16% because of the twinning effect. Based on earlier work of Reyes-Morel and Chen (1988) and Reyes-Morel *et al.* (1988), this part is specified through its rate of change $\dot{f} \langle \boldsymbol{\varepsilon}^{ps} \rangle_{\mathrm{d}V_I}$, which is assumed to depend on the average deviatoric stress $\mathbf{s}^M$ in the matrix according to

$$\langle \boldsymbol{\varepsilon}^{ps} \rangle_{\mathrm{d}V_I} = A \frac{\mathbf{s}^M}{\sigma_e^M}, \quad \sigma_e^M = \sqrt{\frac{3}{2} \operatorname{tr} (\mathbf{s}^M)^2}. \tag{6}$$

Here, A is a material function, which can be considered as a measure of the constraint of the elastic matrix, and σ_e^M is the von Mises stress in the matrix, which will be specified later. When $\sigma_e^M = 0$, A should be put equal to zero because there is no stress bias. The experimental data of Chen and Reyes-Morel (1986, 1987) and Reyes-Morel and Chen (1988) show that under proportional loading the value of A is almost constant during the whole transformation process. Sun *et al.* (1991) have emphasized that (6) is a macroscopic constitutive relationship that is assumed to apply to the ensemble of transformable particles mentioned in the beginning of the section. The deviatoric transformation strain over individual transformed particles will not depend on the local matrix stresses in such a simple manner. First

of all, twinning in a particle will occur in well-defined directions on specific crystallographic planes. Furthermore, the amount of twinning within particles is dependent on particle size (Evans and Cannon, 1986). Although some research has been devoted to nucleation and twinning in a single particle, these are still phenomena that are not well understood and need further attention. However, since in this model many grains with different orientations are considered within dV_I, Sun *et al.* (1991) argue that (6) is an acceptable approximation in the average sense. Combining the expressions (4)–(6), the plastic strain-rate is found as

$$\dot{\mathbf{E}}^p = \dot{f}(\varepsilon^{pd}\mathbf{I} + \langle \boldsymbol{\varepsilon}^{ps} \rangle_{dV_I}). \tag{7}$$

With the help of Eshelby's (1961) solution for an inclusion in an infinite extended elastic body and the method of Mori and Tanaka (1973), the deviatoric and mean matrix stresses, $\mathbf{s}^M$ and σ^M, respectively, are found to be

$$\mathbf{s}^M = \mathbf{S} - fB_1\langle \varepsilon^{ps} \rangle_{V_I}, \quad \sigma_m^M = \Sigma_m - fB_2\varepsilon^{pd}. \tag{8}$$

Here, $\mathbf{S} = \boldsymbol{\Sigma} - \Sigma_m\mathbf{I}$ and $\Sigma_m = \operatorname{tr}\boldsymbol{\Sigma}/3$ are the deviatoric and mean components of the macroscopic stress $\boldsymbol{\Sigma}$, and

$$B_1 = 2G\frac{5\nu - 7}{15(1-\nu)}, \quad B_2 = 2B\frac{2\nu - 1}{1-\nu}, \tag{9}$$

with G the shear modulus, B the bulk modulus and ν Poisson's ratio of the matrix as well as the inclusion, all being related in the standard way to Young's modulus E

$$G = \frac{E}{2(1+\nu)}, \quad B = \frac{E}{3(1-2\nu)}. \tag{10}$$

Equation (6) can be combined with the elastic law $\mathbf{E}^e = \mathbf{M}^0\boldsymbol{\Sigma}$ to yield the macroscopic stress rate–strain rate relation

$$\dot{\mathbf{E}} = \dot{\mathbf{E}}^e + \dot{\mathbf{E}}^p = \mathbf{M}^0\dot{\boldsymbol{\Sigma}} + \dot{f}(\varepsilon^{pd}\mathbf{I} + \langle \boldsymbol{\varepsilon}^{ps} \rangle_{dV_I}) \tag{11}$$

with $\mathbf{M}^0 = (\mathbf{L}^0)^{-1}$ the inverse of the tensor $\mathbf{L}^0$ of elastic moduli of inclusions and matrix. In inverted form, and employing Cartesian components, we then have

$$\dot{\Sigma}_{ij} = 2G(\dot{E}_{ij} - \dot{E}_m\delta_{ij}) + 3B\dot{E}_m\delta_{ij} - \dot{f}(3B\varepsilon^{pd}\delta_{ij} + 2G\langle \varepsilon_{ij}^{ps} \rangle_{dV_I}), \tag{12}$$

where $\dot{E}_m = \dot{E}_{kk}/3$. For future reference, we note that for plane strain conditions, $E_{33} = E_{13} = E_{23} = 0$, so that eqns (11) and (12) reduce to

$$\dot{E}_{\alpha\beta} = \frac{1}{2G}(\dot{\Sigma}_{\alpha\beta} - \nu\dot{\Sigma}_{\mu\mu}\delta_{\alpha\beta}) + (1+\nu)\dot{f}\varepsilon^{pd}\delta_{\alpha\beta} + \dot{f}(\langle \varepsilon_{\alpha\beta}^{ps} \rangle_{dV_I} - \nu\langle \varepsilon_{\mu\mu}^{ps} \rangle_{dV_I}\delta_{\alpha\beta}) \tag{13}$$

and

$$\dot{\Sigma}_{\alpha\beta} = 2G(\dot{E}_{\alpha\beta} - \tfrac{1}{3}\dot{E}_{\mu\mu}\delta_{\alpha\beta}) + B\dot{E}_{\mu\mu}\delta_{\alpha\beta} - \dot{f}(3B\varepsilon^{pd}\delta_{\alpha\beta} + 2G\langle \varepsilon_{\alpha\beta}^{ps} \rangle_{dV_I}) \tag{14}$$

$$\dot{\Sigma}_{33} = -\tfrac{2}{3}G\dot{E}_{\mu\mu} + B\dot{E}_{\mu\mu} - \dot{f}(3B\varepsilon^{pd} + 2G\langle \varepsilon_{33}^{ps} \rangle_{dV_I}) \tag{15}$$

$$\dot{\Sigma}_m = B(\dot{E}_{\mu\mu} - 3\dot{f}\varepsilon^{pd}) = \frac{1+\nu}{3}\dot{\Sigma}_{\mu\mu} - \frac{E}{3}\dot{f}\varepsilon^{pd} + \frac{E}{3}\dot{f}\langle \varepsilon_{\mu\mu}^{ps} \rangle_{dV_I}. \tag{16}$$

The constitutive equations have to be completed by specifying the transformation

condition and the evolution relation in terms of $\dot{f}$. Sun *et al.* (1991) give the following condition for forward transformation to occur

$$F_+(\boldsymbol{\Sigma}, f, T, \langle \varepsilon^{ps} \rangle_{V_t}) = \tfrac{2}{3} A \sigma_e^M + 3\sigma_m^M \varepsilon^{pd} - C_0(T, f) = 0. \tag{17}$$

The function $C_0(T, f)$ depends on the dissipation D_0 (due to interface friction, for instance), on the difference in surface energy A_0, on the free chemical energy difference $\Delta G_{t\to m}(T)$ associated with the transformation (which depends on the temperature T), and on the elastic energy associated with the interaction between transformed particles and matrix

$$C_0(T, f) = D_0 + A_0 + \Delta G_{t\to m}(T) - \tfrac{1}{3} B_1 A^2 - \tfrac{3}{2} B_2 (\varepsilon^{pd})^2 + \alpha B_0 (\varepsilon^{pd})^2 f. \tag{18}$$

The last term in (18) is introduced to incorporate the common experimental observation that the resistance to transformation tends to increase with increasing volume fraction of transformed material; here, this "hardening" is governed by the parameter α. Note that this hardening term is due to processes on microstructural scale, such as (i) particle size dependence: it takes a higher stress level to transform smaller particles; (ii) crystallographic orientation: favourably oriented planes transform first, and (iii) the mutual interference of transformed regions: transformation of a particle will cause a relaxation of the stresses in its surrounding. As the constitutive model is derived for the macroscopic scale, considering many transformable particles in one constitutive element, the hardening effect did not follow from the derivation itself and Sun *et al.* (1991) introduced the last term in (18) on mere phenomenological grounds. The parameter B_0 in (18) is a bulk modulus-like parameter defined by

$$B_0 = \frac{4G(1+\nu)}{1-\nu} + \frac{Gh_0^2(28-20\nu)}{5(1-\nu)} \tag{19}$$

in terms of the parameter

$$h_0 \equiv A/(3\varepsilon^{pd}). \tag{20}$$

The latter parameter will be convenient to use in connection with the shear strain constitutive equation (6), as it relates the strength of the shear strains to the constant dilatation ε^{pd}

$$\sqrt{\tfrac{1}{2} \operatorname{tr} \langle \boldsymbol{\varepsilon}^{ps} \rangle_{dV_t}^2} = \sqrt{3} h_0 \varepsilon^{pd}. \tag{21}$$

Reverse transformation ($m \to t$) can be described by replacing $C_0(T, f)$ in eqn (17) by $\tilde{C}_0(T, f)$, where

$$\tilde{C}_0(T, f) = C_0(T, f) - 2D_0. \tag{22}$$

Even though some authors (e.g. Marshall and James, 1986) report the possibility of reversible transformation, it is not quite clear if reverse transformation takes place in the wake of a crack where unloading occurs. Here, for simplicity, we will assume the transformation is to be irreversible.

The condition (17) furnishes a "transformation surface" in stress space ($\boldsymbol{\Sigma}$) within which transformation is excluded, similar to a yield surface in the usual theory of plasticity. When the transformation proceeds, the transformation surface expands in stress space as well as translates. Borrowing further notions from plasticity theory, the present material with transformation plasticity may be regarded to exhibit mixed hardening; isotropic expansion as a function of f is governed through $C_0(T, f)$, while kinematic hardening originates from the internal stresses appearing in the relations (8) between the matrix stresses and the macroscopic stresses. Moreover, the plastic strain-rate $\dot{\mathbf{E}}^p$ according to (6)

turns out to be normal to the transformation surface in $\boldsymbol{\Sigma}$-space, which is a direct consequence of the model assumptions. The proportionality factor is given by $\dot{f}$, so that

$$\dot{\mathbf{E}}^p = \dot{f}\frac{\partial F_+}{\partial \boldsymbol{\Sigma}}. \tag{23}$$

The growth rate of the fraction transformed tetragonal phase, $\dot{f}$, follows from the consistency condition $\dot{F}_+ = 0$, and is found as

$$\dot{f} = \frac{\langle \boldsymbol{\varepsilon}^{ps} \rangle_{\mathrm{d}V_I} \cdot \dot{\mathbf{S}} + 3\varepsilon^{pd}\dot{\Sigma}_m}{\frac{2}{3}B_1 A^2 + (3B_2 + \alpha B_0)(\varepsilon^{pd})^2}. \tag{24}$$

Expression (24) holds as long as the transformation progresses, i.e. when the current stress state satisfies the transformation condition (17) while there is still a transformable fraction left, $f < f^m$, and no unloading takes place; this is called the loading or transformation branch. When the response is elastic, either because the criterion (17) is not satisfied, $F_+ < 0$, or because elastic unloading occurs from a plastic state, $F_+ = 0$ and $\dot{f} < 0$ according to (24), we must set $\dot{f} = 0$. In summary

$$\dot{f} = \begin{cases} \dfrac{\langle \boldsymbol{\varepsilon}^{ps} \rangle_{\mathrm{d}V_I} \cdot \dot{\mathbf{S}} + 3\varepsilon^{pd}\dot{\Sigma}_m}{\frac{2}{3}B_1 A^2 + (3B_2 + \alpha B_0)(\varepsilon^{pd})^2} & \text{when} \quad F_+ = 0 \quad \text{and} \quad \dot{f} > 0 \\ & \text{when} \quad F_+ < 0 \\ 0 & \text{or} \quad F_+ = 0 \quad \text{and} \quad \dot{f} < 0 \\ & \text{or} \quad F_+ = 0 \quad \text{and} \quad \dot{f} = 0. \end{cases} \tag{25}$$

Finally, the constitutive equations will be rearranged into a form which is necessary for the subsequent numerical analysis. With the relation (11) between strain rates and stress rates, and introducing the following definitions

$$\mathbf{T} \equiv \varepsilon^{pd}\mathbf{I} + A\frac{\mathbf{s}^M}{\sigma_e^M} \quad \text{and} \quad g \equiv \tfrac{2}{3}B_1 A^2 + 3B_2(\varepsilon^{pd})^2 + \alpha B_0(\varepsilon^{pd})^2 \tag{26}$$

one can derive the following rate constitutive equations

$$\dot{\boldsymbol{\Sigma}} = \mathbf{L}\dot{\mathbf{E}}, \tag{27}$$

where the tensor of instantaneous moduli $\mathbf{L}$ is defined by

$$\mathbf{L} = \begin{cases} \mathbf{L}^0 - \dfrac{1}{g}\dfrac{\mathbf{L}^0\mathbf{T} \otimes \mathbf{T}\mathbf{L}^0}{1 + \dfrac{1}{g}(\mathbf{T} \cdot \mathbf{L}^0\mathbf{T})} & \text{when} \quad F_+ = 0 \quad \text{and} \quad \dot{f} > 0 \\ \mathbf{L}^0 & \text{when} \quad F_+ \neq 0 \quad \text{or} \quad \dot{f} < 0. \end{cases} \tag{28}$$

Details may be found in Stam (1992). On the transformation branch, the stiffness tensor $\mathbf{L}$ is comprised of the linear elastic stiffness tensor $\mathbf{L}^0$ and a nonlinear part due to the transformation which is similar to the well-known plastic moduli in elastoplasticity. It is of considerable importance to note that the moduli $\mathbf{L}$ possess the following symmetry when expressed in their Cartesian components L_{ijkl}

$$L_{ijkl} = L_{klij} \tag{29}$$

in addition to the obvious symmetries in ij and kl.

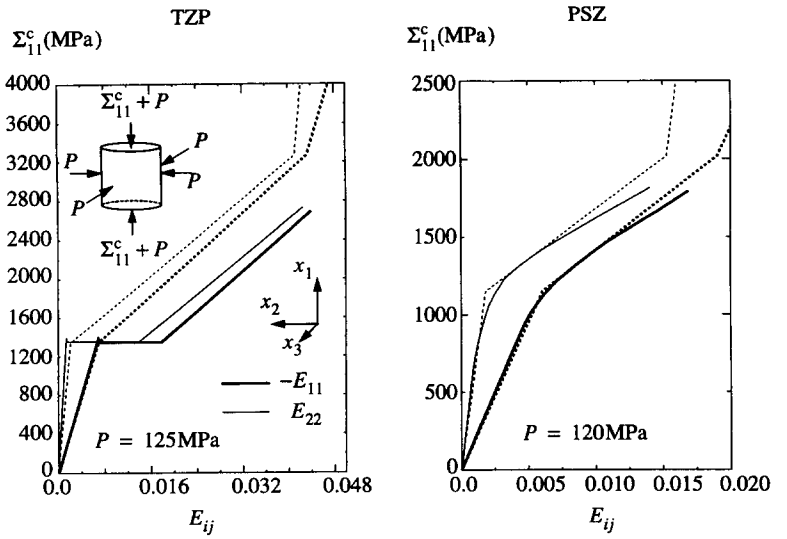

Fig. 1. Stress–strain curves for TZP and PSZ obtained by triaxial compression at room temperature. The dashed lines give the response of the constitutive model.

Comparison with experiments

To illustrate the capabilities of the model, in Fig. 1 the predicted stress–strain relations are compared with experimental stress–strain curves for TZP and PSZ materials. The experimental data were obtained under triaxial compression by Reyes-Morel and Chen (1988) and Chen and Reyes-Morel (1986), respectively. The dashed lines show the theoretical response in the axial (x_1) and radial (x_2 and x_3) directions. The strain in the axial direction is negative and the strains in the radial directions are positive. Obviously, plastic strains of that nature cannot be described by a purely dilatant model.

For both materials we used $E = 190$ MPa, $\nu = 0.3$ (taken from the above-mentioned papers) and $\varepsilon^{pd} = 0.015$. The remaining material parameters for TZP are estimated to be $f^m = 1$, $\alpha = 1.16$, $h_0 = 1.3$ and with the critical transformation stress under compression $\Sigma^{cc}_{11} = 13 \times 10^2$ MPa (estimated from Fig. 1) and the hydrostatic pressure $P = 125$ MPa, it follows from the transformation condition (17) that prior to transformation, $C_0(T_0, 0) = 30$ MPa at constant temperature T_0. For convenience we define $C_0 \equiv C_0(T_0, 0)$. For PSZ the remaining parameters are estimated to be $f^m = 0.35$, $\alpha = 1.2$, $h_0 = 1.3$ and $C_0 = 22$ MPa (based on $\Sigma^{cc}_{11} = 11.5 \times 10^2$ MPa and $P = 120$ MPa from Fig. 1).

For the TZP material experiments suggest a nearly perfectly plastic regime just after initiation of transformation which later turns into a region were linear hardening is observed. This bilinear transformation behaviour in TZP cannot be modelled with the present model and the representation in Fig. 1 uses linear hardening immediately after transformation. For PSZ we see that in the experiment the transition from linear elasticity to transformation plasticity occurs more gradually, whereas in the theoretical model the transition is sharp. Note that in theory, the response becomes linear elastic again once the transformation is completed, whereas in the experiment specimens fail before reaching complete transformation.

We may conclude that compared to the capabilities of the dilatant model, the general material behaviour is described much better: in the triaxial compression test, negative transformation strains develop in the axial direction due to the influence of the shear component. The model is capable of following the general trend of the experimentally derived stress–strain relation, however, more detailed material characteristics, like the nearly perfectly-plastic regime just after initiation of transformation for TZP, are not (yet) captured.

Relation to the dilatant transformation model

When the material function A in (6) vanishes, so that $h_0 = 0$ according to (20), the phase transition involves pure dilatation only and the macroscopic shear response is entirely

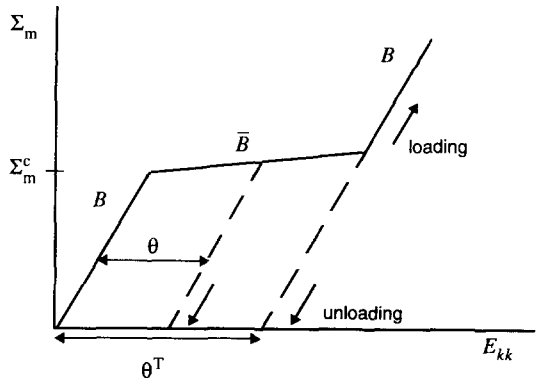

Fig. 2. Macroscopic mean stress dilatation response when the transformation is purely dilatant, $h_0 = 0$.

linear elastic. Indeed, the above model then reduces to that given by Budiansky *et al.* (1983). With reference to the general expressions (11), (12), the dilatant stress–strain behaviour of the composite with $A = h_0 = 0$ can be directly written as

$$E_{kk} = \frac{\Sigma_m}{B} + \theta, \tag{30}$$

where the current volumetric transformation strain parameter θ introduced by Budiansky *et al.* (1983) can be expressed in terms of the volume fraction f and the transformation dilatation ε^{pd} as $\theta = 3f\varepsilon^{pd}$. This behaviour is illustrated in Fig. 2. When the material is partially transformed, i.e. $f < f^m$, the growth rate of f is found from (24) as

$$\dot{f} = \frac{3}{(3B_2 + \alpha B_0)} \frac{\dot{\Sigma}_m}{\varepsilon^{pd}} \tag{31}$$

in terms of the hardening parameter α. Budiansky *et al.* (1983) characterize that same behaviour through the relation

$$\dot{\theta} = \left(1 - \frac{\bar{B}}{B}\right)\dot{E}_{pp}, \tag{32}$$

where $\bar{B}$ can be directly interpreted as the bulk modulus of the intermediate segment of the stress–strain curve of Fig. 2 where transformation occurs. Stam (1992) has shown the following relationship between α and $\bar{B}$

$$\alpha = \frac{9B\bar{B} - 3BB_2 + 3B_2\bar{B}}{BB_0 - B_0\bar{B}} \quad \text{or} \quad \bar{B} = \frac{B(B_2 + \frac{1}{3}\alpha B_0)}{B_2 + \frac{1}{3}\alpha B_0 + 3B}. \tag{33}$$

3. LOSS OF ELLIPTICITY DUE TO TRANSFORMATION

The hydrostatic stress–mean strain response shown in Fig. 2 for purely dilatant behaviour exhibits softening in the intermediate segment where transformation occurs when $\bar{B} < 0$. Budiansky *et al.* (1983) pointed out that when $\bar{B} < -4G/3$, the incremental governing equations cease to be elliptic, thus enabling discontinuities in the stress and strain fields. In that case, discontinuities may also occur in θ so that if $\bar{B} \leqslant -4G/3$, all particles can transform spontaneously and completely to the maximal value $\theta^T = 3f^m\varepsilon^{pd}$. Accordingly, they designated materials with $\bar{B} < -4G/3$ as supercritically transforming materials, while subcritical materials are characterized by $\bar{B} > -4G/3$. In the latter case, the governing

equations remain elliptic and the material can exist in a stable partially transformed state, $\theta < \theta^T$.

In this section, we wish to explore these different ranges of material behaviour for the more general model for transforming composite materials of Section 2. We shall do so by considering the possibility that the associated governing equations lose ellipticity, making use of the observation that, for a class of constitutive equations of the type (27)–(29), this coincides with the onset of localization (e.g. Rice, 1976). In contrast to the situation considered by Budiansky *et al.* (1983), loss of ellipticity is no longer a material characteristic alone, but depends also on the current state. Hence, we will have to adopt the term subcritical in a more narrow sense for materials that, under a given macroscopically homogeneous state of deformation or stress, exclude loss of ellipticity. Nevertheless, it is of importance to know which combination of material parameters may lead to localization during a certain deformation history.

In view of the forthcoming crack growth analyses, we will consider small strain deformation histories under plane strain conditions. Following Rice (1976), for example, and adopting in particular the procedure outlined by Ortiz *et al.* (1987), the onset of localization is considered as a bifurcation phenomenon from homogeneous deformations into a deformation field that is discontinuous across a plane with unit normal vector **n**. The onset of localization can then be established by considering the so-called localization (or acoustic) matrix **A**(**n**) defined by

$$\mathbf{A}(\mathbf{n}) \equiv \mathbf{nLn} \tag{34}$$

in terms of the current values of the moduli **L**. For localization to occur, the matrix **A**(**n**) has to have at least one zero eigenvalue, which necessitates

$$f(\mathbf{n}) = \det(\mathbf{A}(\mathbf{n})) = 0. \tag{35}$$

For plane strain, the localization matrix is a 2×2 matrix and one readily finds that the determinant of the acoustic matrix $\det(\mathbf{A}(\mathbf{n})) = a_0 n_1^4 + a_1 n_1^3 n_2 + a_2 n_1^2 n_2^2 + a_3 n_1 n_2^3 + a_4 n_2^4$, where the coefficients $(a_0, \ldots, a_4)$ depend on the various components of the current moduli **L** (see Ortiz *et al.*, 1987). Setting $n_1 = \cos\theta$ and $n_2 = \sin\theta$ the localization condition becomes

$$f(x) = a_4 x^4 + a_3 x^3 + a_2 x^2 + a_1 x + a_0 = 0, \tag{36}$$

where $x = \tan\theta$. Hence, the onset of localization is signaled with a real-valued solution of (36) can be found, which then immediately gives the orientation of the localization plane.

As a check on this procedure, we shall first briefly reconsider the loss of ellipticity for the model with purely dilatant transformations as summarized in eqns (30)–(33). In this case, the shear part of the macroscopic response is entirely linear elastic. Therefore, to detect localization, we only need to consider purely dilatant deformation paths. For various values of $\bar{B}$, we scan the total mean stress–dilatancy path of Fig. 2 by incrementally increasing the dilatancy. For each increment the current values of the components of **L** are used to compute the coefficients $(a_0, \ldots a_4)$ to be substituted into the localization condition (36). Evidently, in the linear-elastic branches, no localization is found; but, on the intermediate branch where transformation takes place, it is found that localization occurs if $\bar{B} \leqslant -4G/3$, or, with (33), if $\alpha \leqslant 0$. This agrees completely with the results of Budiansky *et al.* (1983).

Next the shear effects of the phase transformation will be taken into account as well ($h_0 \neq 0$). To detect the possible occurrence of localization, again we will scan the total stress–strain path for a number of values for α and h_0, but now we also need to specify the direction of the deformation path in strain-space. Assuming plane strain situations, we will do so by considering proportional incremental deformation paths in $E_{\alpha\beta}$-space. To get a reasonably complete picture of the behaviour, we cover a rather wide range of directions by prescribing the various ratios of incremental principal strains. The ratio $\rho = \Delta E_{22}/\Delta E_{11}$ will be varied within the range $[-1, 1]$.

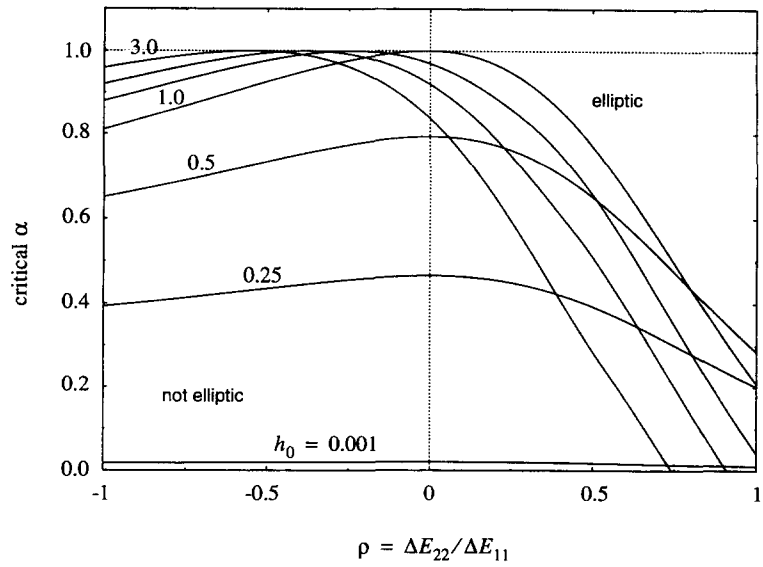

Fig. 3. The critical value of the hardening parameter α for which, with various values of $h_0 \in \{0.001, 0.25, 0.5, 1, 1.5, 2, 3\}$, ellipticity is lost during a proportional deformation path specified by $\rho = \Delta E_{22}/\Delta E_{11}$ under plane strain conditions.

For chosen values of h_0 and ρ (and $\nu = 0.3$), the critical hardening parameter α at which localization can occur has been determined numerically from (36) in a similar fashion as discussed above. In Fig. 3 the critical values of α are plotted as a function of the strain ratio $\rho \in [-1, 1]$ for various values of h_0. The curve for each value of h_0 separates the elliptic region from the non-elliptic region. Above each curve, localization is prohibited and ellipticity of the equations is ensured; for values of α below the curve, localization will develop as soon as the transformation is initiated. Borrowing the Budiansky *et al.* (1983) terminology, the curves in Fig. 3 thus separate the supercritical transformation regimes from the subcritical regimes in which the transformation process develops gradually; but, it should be remembered that this holds essentially only for the plane strain proportional deformations considered here.

From Fig. 3 it is seen that, when h_0 is reduced to zero, the critical value of α asymptotically reduces to $\alpha = 0$, independent of the strain ratio ρ. This confirms the earlier result for the purely dilatant model. If the transformation shear effects are not neglected ($h_0 \neq 0$), it can be seen that for ellipticity to be guaranteed for an increasing influence of the transformation shear effects, i.e. increasing values of h_0, the hardening parameter α must be increased. For increasing values of h_0, and for negative values of ρ, the critical hardening parameter α tends to approach the value unity. However, it should be noted that with increasing values of h_0, the model is increasingly sensitive to nonproportional loading histories; but here, no attempt has been made to investigate the influence of nonproportional loading histories. Nevertheless, the results suggest that a value of $\alpha \geqslant 1$ will probably be large enough to avoid localization. All crack growth results to be presented later have used values for α in this range. Experimental results described by Sun *et al.* (1991) indicate values $h_0 = 1.4$ and $\alpha = 1.16$ for TZP materials, and $h_0 = 1.3$, $\alpha = 1.2$ for PSZ materials. Clearly, these values fall in the elliptic/subcritical regimes of Fig. 3.

4. FORMULATION OF THE CRACK GROWTH PROBLEM

In this section we turn to the study of the fracture toughening caused by the phase transition, using the constitutive model of Section 2. The particular transient crack growth problem that we use, is similar in many aspects to that studied by Hom and McMeeking (1990). The present exposition of its formulation will therefore be rather brief, and focus mainly on the novel aspects associated with the shear transformation strain effects.

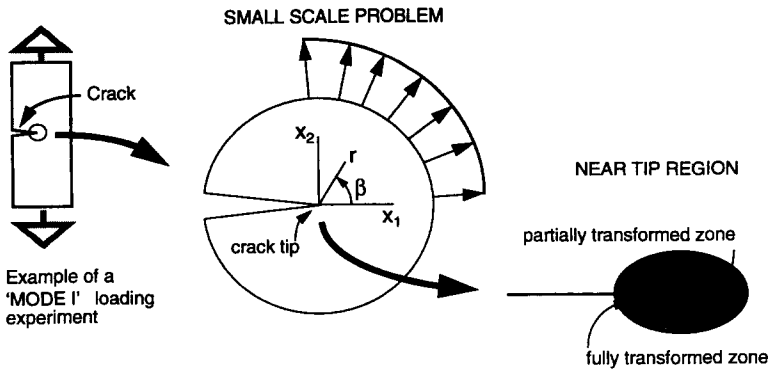

Fig. 4. The small scale transformation assumption and the corresponding boundary-value problem for a semi-infinite crack subjected to a mode I opening mode.

As stated in Section 2, the induction of the transformation of tetragonal zirconia requires a certain critical stress level. Because of the high stresses that develop in the neighbourhood of the crack tip, the material near the crack tip will undergo the transformation, but the height of the transformation zone will remain small compared to the length a of the crack (Rühle and Evans, 1989). Under this small scale transformation condition, the stress field remote from the tip is not disturbed by the transformation strains and an asymptotic problem can be formulated for a semi-infinite crack (see Fig. 4). Under mode I loading and plane strain conditions, the stress field remote from the tip is given by

$$\Sigma_{ij} = \frac{K^{\mathrm{APP}}}{\sqrt{2\pi r}} f_{ij}(\theta), \quad r \to \infty, \tag{37}$$

where K^{APP} is the elastic stress intensity factor which will be referred to as the applied stress intensity factor, and where the $f_{ij}(\theta)$ are the universal dimensionless angular functions. Thus, a domain Ω can be considered where the displacement boundary conditions can be prescribed by using the linear elastic relations, if the applied stress intensity factor K^{APP} is known.

As the tip of the crack is approached, the transformation zone is encountered, and the stress field is disturbed by the transformation strains. In the immediate vicinity of the crack tip, a zone of completely transformed material ($f = f^m$) will be present, surrounded by a zone of partially transformed material ($f < f^m$). Inside the fully transformed zone, the incremental response of the material is again linear elastic, so that the stress field has precisely the same form as in (37) but with a different intensity factor K^{TIP}, i.e.

$$\Sigma_{ij} = \frac{K^{\mathrm{TIP}}}{\sqrt{2\pi r}} f_{ij}(\theta), \quad r \to 0. \tag{38}$$

It is assumed that K^{TIP} governs the fracture process near the tip, so that the crack advances when $K^{\mathrm{TIP}} = K^{\mathrm{C}}$, the fracture toughness of the composite at the crack front. Because of the transformation, K^{TIP} and K^{APP} will differ by an amount ΔK^{TIP} defined by

$$K^{\mathrm{TIP}} = K^{\mathrm{APP}} + \Delta K^{\mathrm{TIP}}, \tag{39}$$

where $\Delta K^{\mathrm{TIP}} < 0$ if shielding occurs due to the transformation strains.

It is the reduction from K^{APP} to K^{TIP} that determines the toughness enhancement due to transformation. Obviously, when no transformation occurs $K^{\mathrm{TIP}} = K^{\mathrm{APP}}$. If transformation strains start to develop under monotonically increasing K^{APP}, even while there is no crack growth yet, then in general $K^{\mathrm{TIP}} \neq K^{\mathrm{APP}}$. Budiansky *et al.* (1983) showed, however, that for the purely dilatant model the conclusion $K^{\mathrm{TIP}} = K^{\mathrm{APP}}$ is retained prior to crack propagation

on the basis of the path-independence of the J-integral (Rice, 1968). The proof relies on the observation that the dilation at each point will increase monotonically as K^{APP} is increased, so that the transformation-induced inelastic behaviour can be approximated by a nonlinear elastic set of constitutive equations, for which the path-independency of the J-integral still holds (Turner, 1979). This conclusion does not apply to the more general, incremental constitutive model of Sun *et al.* (1991) that was discussed in Section 2. Because of the stress redistributions in the vicinity of the crack tip that will accompany the phase transformations, the deformation path of a material point does not remain proportional. Hence, even when the unloading response can be disregarded, the actual response cannot be replaced with a nonlinear elastic response as in the purely dilatant case. Therefore, it must be concluded that, with the constitutive model of Sun *et al.* (1991), the initial transformation zone, i.e. prior to crack growth, may already influence the toughness. This will be demonstrated further in Section 6.

If K^{TIP} reaches the critical stress intensity K^C, the crack propagates and a wake of transformed material is formed. K^{TIP} decreases relative to K^{APP}, so that in order to maintain crack growth, K^{APP} must be continually adjusted so that K^{TIP} equals the critical value K^C. Although the intrinsic material toughness does not change, the effective toughness is given by K^{APP} and will in general be a function of the crack advance Δa. The relative toughness increase is defined by $K^{APP}/K^{TIP} = 1 - \Delta K^{TIP}/K^C$. In the present paper, the toughening effect will be computed by a slight extension of a method discussed by McMeeking and Evans (1982) and Budiansky *et al.* (1983). The near-tip intensity reduction ΔK^{TIP} is obtained by integration over the upper half Ω of the transformed zone, of the intensity enhancement dK^{TIP} under plane strain mode I conditions due to two "spots" of infinitesimal area dA undergoing a transformation strain:

$$\Delta K^{TIP} = \int\int_{\Omega} dK^{TIP}. \tag{40}$$

One of the spots is located at (r, β) (see Fig. 4) with respect to the crack tip, and is characterized by the in-plane stress-free transformation strains E^p_{11}, E^p_{22}, E^p_{12}, while the second is located symmetrically with respect to the crack plane at $(r, -\beta)$, and undergoes stress-free transformation strains E^p_{11}, E^p_{22}, $-E^p_{12}$. The explicit form of dK^{TIP} under conditions of plane stress has been given by Hutchinson (1974). When we neglect higher order terms and enforce plane strain conditions [see also Budiansky *et al.* (1983)], it follows that

$$dK^{TIP} = \frac{1}{\sqrt{8\pi}} \frac{E}{(1-\nu^2)} r^{-3/2} M(E^p_{\alpha\beta}, \beta)\, dA, \tag{41}$$

where

$$M(E^p_{\alpha\beta}, \beta) = (E^p_{11} + E^p_{22}) \cos\frac{3\beta}{2} + 3E^p_{12} \cos\frac{5\beta}{2} \sin\beta + \frac{3}{2}(E^p_{22} - E^p_{11}) \sin\beta \sin\frac{5\beta}{2} \tag{42}$$

[see also Lambropoulos (1986)]. The transformation strains $E^p_{\alpha\beta}$ to be substituted into for the present situation are the in-plane transformation strains that would occur under plane strain conditions but without in-plane stresses, i.e. $\Sigma_{\alpha\beta} = 0$ with $E_{i3} = 0$. With the general three-dimensional transformation strain $\mathbf{E}^p$ in each spot being given by (2), it follows from the plane strain expressions (13) that the resulting nonzero strains are given by

$$\begin{aligned} E^p_{11} &= (1+\nu) f\varepsilon^{pd} + f[\langle \varepsilon^{ps}_{11} \rangle_{V_t} - \nu(\langle \varepsilon^{ps}_{11} \rangle_{V_t} + \langle \varepsilon^{ps}_{22} \rangle_{V_t})] \\ E^p_{22} &= (1+\nu) f\varepsilon^{pd} + f(\langle \varepsilon^{ps}_{22} \rangle_{V_t} - \nu(\langle \varepsilon^{ps}_{11} \rangle_{V_t} + \langle \varepsilon^{ps}_{22} \rangle_{V_t})) \\ E^p_{12} &= f\langle \varepsilon^{ps}_{12} \rangle_{V_t} \end{aligned} \tag{43}$$

which can also be found in Lambropoulos (1986). The transition of the mode I experiment to a small scale problem, as illustrated in Fig. 4, implies the loss of the crack length a as an

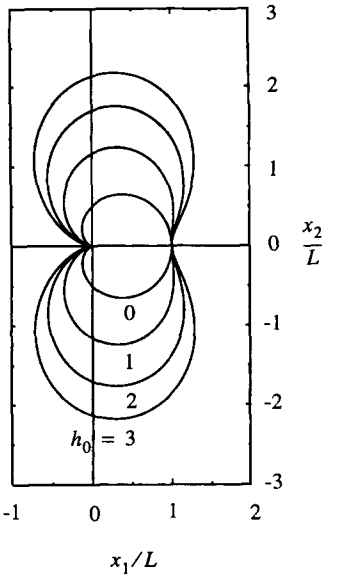

Fig. 5. The shape of the transformation zone, normalized by the length parameter L for various values of h_0.

explicit length scale which is then implicitly prescribed in K^{APP}. To normalize all length scales, we use the parameter L defined by

$$L = \frac{2}{9\pi}\left[\frac{K^{\mathrm{C}}\{h_0(1-2\nu)+(1+\nu)\}}{\Sigma^c}\right]^2 \tag{44}$$

with

$$\Sigma^c = C_0(T)/(3\varepsilon^{pd}). \tag{45}$$

Physically, L is the distance on the axis in the direction of the crack, from the tip to the boundary of the transformation zone, when it is assumed that the transformation strains are so small that they do not disturb the elastic stress field. This approximate transformation zone is then readily obtained by substituting the unperturbed stress field into the transformation criterion (17), which then reduces to

$$\tfrac{2}{3}h_0\Sigma_e + \Sigma_m = \Sigma^c \tag{46}$$

[for more details see Stam (1992)]. This expression emphasizes that the parameter h_0 governs the influence of the shear transformation strains and, as a result, the shape of the (initial) transformation zone. The approximate initial transformation zones thus found are shown in Fig. 5 for various values of h_0. If $h_0 = 0$, then the constitutive model reduces to the dilatant model and the definition of L given in (44) reduces to the one by Hom and McMeeking (1990). For this special case, the shape of the transformation zone was already determined by McMeeking and Evans (1982). If the value of h_0 is increased the height of the transformation zone, when scaled with the parameter L, is increased, and also the shape changes.

Finally, the solutions depend on the strength of the transformation, which will be characterized by the same nondimensional parameter ω as used by Hom and McMeeking (1990)

$$\omega = \frac{3Ef^m\varepsilon^{pd}}{\Sigma^c}\left[\frac{1+\nu}{1-\nu}\right]. \tag{47}$$

Notice that this parameter is not modified for the additional effect of transformation shear strains, because their intensity is related to ε^{pd}, see (6) and (20).

5. FINITE ELEMENT ANALYSIS

A displacement-based finite element method is used to solve the boundary-value problem described in the previous section. Extensive use is made of the fact that the constitutive equations for the Sun *et al.* (1991) transformation model have been cast in a form [eqns (27) and (28)] that is completely similar to the usual time-independent elasto-plasticity equations with an associative flow rule. In that case the parameter time, t, may be replaced by any other monotonically increasing parameter; here time is replaced by K^{APP}. The resulting finite element equations for the displacement rates are then solved in a linear incremental manner. In each increment i, the nodal displacement increments $\Delta\mathbf{u}^{(i)}$ are solved from

$$\mathbf{K}^{(i)}\Delta\mathbf{u}^{(i)} = \Delta\mathbf{F}^{(i)} - (\mathbf{D}^T\boldsymbol{\Sigma}^{(i)} - \mathbf{F}^{(i)}), \quad \text{with } \mathbf{K}^{(i)} = \mathbf{D}^T\mathbf{S}^{(i)}\mathbf{D}, \tag{48}$$

where $\Delta\mathbf{F}^{(i)}$ is the vector of nodal load increments and where the stiffness matrix $\mathbf{S}^{(i)}$ is determined by the instantaneous moduli $\mathbf{L}$ appearing in (27). The bracket term on the right-hand side of (48) is an equilibrium correction based on the current discrete stress state, collected formally in the vector $\boldsymbol{\Sigma}^{(i)}$. With these $\Delta\mathbf{u}^{(i)}$, the state in each integration point is updated in the usual manner for geometrically linear elastoplasticity problems. If after some loading the critical stress level is reached so that the transformation criterion $F_+ = 0$ is satisfied, the incremental volume fraction of transformed material $\Delta f^{(i)}$ can be found from the incremental version of (25). It is emphasized that, in contrast to the situation in case of the purely dilatant model of Budiansky *et al.* (1983), the current transformation strain will have to be determined incrementally as well. The deviatoric part deserves special attention. With $\langle\boldsymbol{\varepsilon}^{ps}\rangle^{(i)}_{\mathrm{d}V_t}$ being determined from the current stresses $\mathbf{s}^M_{(i)}$ according to (6), the incremental change of $\mathbf{E}^{ps}$ is obtained from (7) as

$$\mathbf{E}^{ps}_{(i+1)} = \mathbf{E}^{ps}_{(i)} + \Delta\mathbf{E}^{ps}_{(i)}, \quad \text{with } \Delta\mathbf{E}^{ps}_{(i)} = \Delta f^{(i)}\langle\boldsymbol{\varepsilon}^{ps}\rangle^{(i)}_{\mathrm{d}V_t}. \tag{49}$$

On the other hand, according to (3) we also have $\mathbf{E}^{ps}_{(i+1)} = f^{(i+1)}\langle\varepsilon^{ps}_{ij}\rangle^{(i+1)}_{V_t}$ from which we can compute the deviatoric components of the particle transformation strain as

$$\langle\boldsymbol{\varepsilon}^{ps}\rangle^{(i+1)}_{V_t} = \frac{f^{(i)}\langle\boldsymbol{\varepsilon}^{ps}\rangle^{(i)}_{V_t} + \Delta f^{(i)}\langle\boldsymbol{\varepsilon}^{ps}\rangle^{(i)}_{\mathrm{d}V_t}}{f^{(i+1)}}. \tag{50}$$

In our analysis, about 100 loading increments ΔK^{APP} are applied to reach the critical value K^{C} at the crack tip. This turned out to be necessary to accurately describe the development of the initial transformation zone, and in particular to account adequately for the nonproportional stress changes that accompany the resulting stress redistributions inside and in the vicinity of the expanding transformation zone. Furthermore, on the transformation branch of the constitutive response, ten subincrements are taken within each increment in order to be able to take relatively large loading increments to save computing time. The incremental loading displacements $\Delta\mathbf{u}$, found from (48), are simply divided into ten equally sized subincremental displacements $\Delta\Delta\mathbf{u}$, which are then used to incrementally calculate the incremental strains and stresses, and also the transformation behaviour, in a similar manner as discussed above. However, if the current stress state is not on the transformation branch, so that the material behaviour is linear elastic, no subincrements are taken in order to reduce computation time. If during an increment the material's response changes from linear elastic to a transformation plasticity response, the

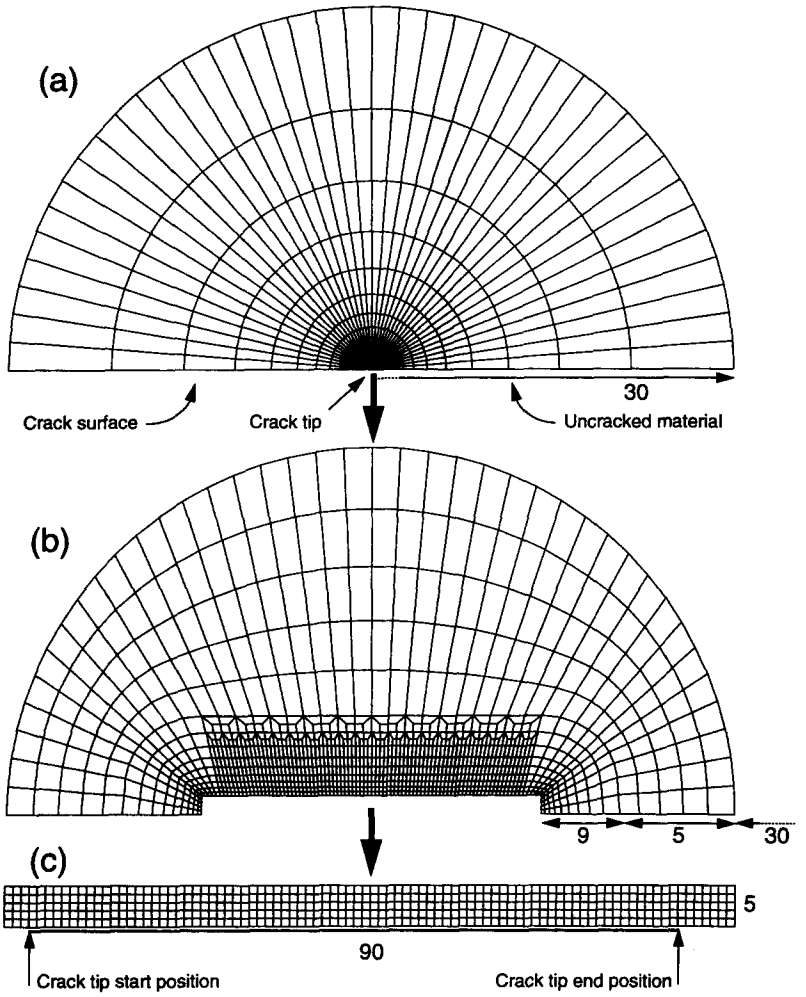

Fig. 6. The finite element mesh used to analyse the small scale crack growth problem.

first subincrement is taken such that the transformation criterion (17) is met exactly, and subsequent subincrements are taken to follow the transformation branch. In case the material's response changes to the linear elastic branch because the transformation is exhausted, $f \geqslant f^m$, the last subincrement on the transformation branch is adjusted such that the updated value of f is exactly equal to the maximum value f^m.

In the finite element analysis, quadrilateral elements are used, each of which is built up of four constant strain elements. The mesh that has been used is shown in Fig. 6, and contains 2770 quadrilateral elements and 2880 nodes. Only the upper half of the small scale region has been considered because of symmetry. Displacement boundary conditions are prescribed on the circular outer boundary. The mesh is designed such that the mesh is highly refined near the tip, as shown in Fig. 6. At the start, the crack tip is placed at three elements to the right of the left-hand side of the rectangular region of the mesh, as shown in Fig. 6(c). Crack growth was permitted over a span of 80 nodes to the right-hand side of the mesh.

The stress intensity at the crack tip, K^{TIP}, is computed numerically on the basis of the integral formulation (40)–(42) by a 13-point Gaussian-integration within each element. Near the crack tip (within a radius of three elements) the integration is carried out analytically to take care of the singularity in (41) at the tip. When this value reaches the critical stress intensity K^{C}, crack growth is simulated by using a nodal release technique comparable to the method used by Hom and McMeeking (1990). The nodal force at the current crack

tip node position is stepped down to zero in five increments, and the displacement boundaries at the outer radius are adjusted to the new position relative to the moved tip.

6. RESULTS

The crack growth problem defined above is characterized by the following parameters: K^{APP}, Δa, L (small-scale transformation problem), E, ν, f^m, ε^{pd}, Σ^c, α, h_0 (deformation response of material) and K^C (fracture process). The numerical results of the refined computations described above to be presented here will focus on the evolution of transformation zones and the toughness increase $K^{APP}(\Delta a)/K^C$ during crack growth. Dimensional analysis reveals that the solution must depend on nondimensional combinations of these parameters, and upon close examination of the governing equations, it follows that these results can be expressed in terms of the following subset of these nondimensional parameters

$$\frac{K^{APP}}{K^C}, \frac{\Delta a}{L}, \nu, \alpha, \omega, h_0. \tag{51}$$

Of course, other combinations may be chosen, but this set turns out to be convenient. Note that this set of parameters is similar to that considered by Hom and McMeeking (1990) but augmented with the parameter h_0 relating the shear transformation strain to the constant lattice dilatation ε^{pd}.

Throughout the analysis we take $\nu = 0.3$ in (51), but various combinations of the other parameters ω, α and h_0 are considered to study their effect on toughening as well as on the size and shape of the transformation zone. Proceeding from the parameter study by Hom and McMeeking (1990), the strength of the transformation is varied from $\omega = 5$ to 10. For each value of ω, the hardening parameter α is chosen to be either 1 or 1.25. The smallest value of the hardening parameter α is chosen to be 1 to avoid localization over a wide range of material parameters, as discussed in detail in Section 3. The value $\alpha = 1.25$ has been chosen as a representative value to cover the experimental values of $\alpha = 1.16$ and 1.2 for TZP and PSZ, respectively, given by Sun *et al.* (1991). For each of the four combinations of these parameters, the influence of the transformation shear is varied by taking $h_0 = 0$, 0.5, 1.0 or 1.5, which covers the experimental values given by Sun *et al.* (1991) for various materials and includes the limit of pure dilatational transformations for comparison. It would have been interesting to perform computations for larger values of ω but the number of variations was limited because of time considerations: a typical crack growth computation up to a steady-state situation required about 95 CPU hours on a SUN Sparc workstation 1.

Before presenting the results of these computations, it is instructive to comment on the way in which the intensity of the transformation shear strains is related to the dilatation ε^{pd}. A convenient parameter to characterize the rate of change of the amount of transformation shear strains in the composite material is

$$\dot{E}_e^{ps} = \sqrt{\tfrac{2}{3}\operatorname{tr}\dot{\mathbf{E}}^{ps2}} = 2\dot{f}h_0\varepsilon^{pd}, \tag{52}$$

where, in the last equality, we have substituted the expressions (6) and (7) to eliminate $\dot{\mathbf{E}}^{ps}$. This can be immediately integrated during the deformation process to find that $E_e^{ps} = 2fh_0\varepsilon^{pd}$, showing that the intensity of the transformation strain only depends on the volume fraction f, since the factor $2h_0\varepsilon^{pd}$ is a constant that for a given value of ε^{pd} depends on the choice of h_0. The maximum value of h_0 should correspond therefore to a material in which no twinning occurs. As already mentioned in Section 2, the stress-free lattice shear strain in ZrO_2 is 16%, so that with $\varepsilon^{pd} = 1.5\%$ it follows that $h_0^{max} \approx 3.08$. The lower bound of h_0 corresponds to a situation where twinning completely eliminates the average shear transformation and $h_0 = 0$. In this case the transformation is purely dilatant and the results agree well with those of Hom and McMeeking (1990). Noting that these authors used a quite

different, iterative rather than an incremental scheme, this agreement gave us confidence in the numerical procedure.

To check the convergence of the solution, some computations with refined meshes have been performed. In this small scale problem, mesh refinement can be obtained simply by increasing the characteristic length L with respect to the dimensions of the smallest element, while leaving all other parameters unchanged. In this way the transformation zone will contain more elements and more accurate results should be obtained, as long as the small scale condition is not violated.

Transformation zones

Since for all chosen material parameters, the material behaviour is subcritical (see Section 3), the transformation varies continuously around the crack tip. In this case, a convenient way to visualize the transformation zones is to plot the distribution of transformed material by means of contours of constant value of the ratio of the transformed fraction compared to the maximum available transformable fraction, f/f^m. No attempt has been made to smoothen the contours, so that, in particular when the transformation zone grows outside the highly refined zone around the crack path, the contours may come out somewhat irregular. The transformation zones for the four combinations of α and ω considered, are shown in Figs 7–10 for various values of h_0. In these plots, the elements in which the material is completely transformed ($f/f^m = 1$) are also shown. For the subsequent discussion, it is convenient to follow experimental practice and define the height of the transformation zone h as the distance in x_2-direction from the crack surface to the point where the fraction of transformed material is 50% ($f/f^m = 0.5$) (see also Fig. 7d).

It is seen that the area around the crack path is fully transformed. Moving further into the material, perpendicular to the crack surface in the x_2 direction, the fully transformed zone is followed by a region of partially transformed material and finally the untransformed material is reached. In general, the zone height increases as the crack grows. From a mechanical point of view, this can be explained by noting that the transformation-plasticity shields the crack tip, so that K^{APP} must be increased to maintain the critical stress intensity at the crack tip, as mentioned before. Increasing the value of K^{APP}, raises the stresses in the elastic field and thus enlarges the region where the critical transformation stress is reached. After some crack growth, however, the initial sharp increase becomes more gradual due to stress redistributions and the zone height reaches a maximum. In the present analyses, the cracks could only grow over a limited distance and in some cases—particularly for larger values of h_0—the maximum value had not yet been attained. In all cases where a steady-state was reached, the steady-state zone height is found to be slightly smaller than the maximum height. Table 1 gives the value of the peak height h of the transformation zone, together with the value $\Delta a/L$ when this peak occurs.

Examination of the results reveals that, in general, the shape and the size of the transformation zones is strongly influenced by whether or not the transformation is near-critical. As discussed in Section 3, this depends on the hardening α, the influence of the shear transformation h_0 and the deformation path. In Fig. 7 for instance, where $\omega = 5$ and $\alpha = 1$, it is observed that contours of f/f^m approach each other for $h_0 = 0.5$ and for $h_0 = 1.0$, as compared to the dilatant case ($h_0 = 0$). This is indicative of near-critical behaviour, and can be explained to a certain extent by consideration of Fig. 3. Knowing from the finite element analyses that in the range $0.5 \leqslant h_0 \leqslant 1.0$, the ratio $\rho = \Delta E_{22}/\Delta E_{11}$ of strain increments in the region where transformation takes place is in the interval $[-0.3, 0.3]$, it is seen that a value $\alpha \geqslant 1$ is really needed around $h_0 = 1.0$ to prevent localization, and thus supercritical behaviour. For $h_0 = 1.5$, the situation is less critical since for this case a hardening of $\alpha = 1$ is only needed for values of $\rho < -0.1$, whereas inside the transformation area, the parameter ρ is found to vary between 0 and 0.6. This results in a much more gradual transition from fully transformed to untransformed for $h_0 = 1.5$.

As for the frontal parts of the transformation zones shown in Figs 7–10, it is seen that the zones enlarge in the x_1 direction with increasing value of h_0, and also that the transformation zone shapes change rather drastically. When the hardening is increased from a value $\alpha = 1$ to 1.25 as shown in Fig. 8, it is observed that for all h_0 the transition

Table 1. Peak values of transformation zone heights and fracture toughnesses

ω	5	5	5	5	5	5	5	5	10	10	10	10	10	10	10	10
α	1	1	1	1	1.25	1.25	1.25	1.25	1	1	1	1	1.25	1.25	1.25	1.25
h_0	0	0.5	1.0	1.5	0	0.5	1.0	1.5	0	0.5	1.0	1.5	0	0.5	1.0	1.5
Peak h/L	0.45	0.78	>0.96	0.79	0.37	>0.64	>0.75	0.70	0.33	0.69	0.78	1.38	0.23	0.46	0.51	0.34
$\Delta a/L$	1.15	3.74	>5.81	3.74	1.00	>4.98	>5.81	1.71	1.00	4.98	>5.81	5.87	0.70	2.99	>5.81	0.57
peak K^{APP}/K^{TIP}	1.19	>1.35	>1.46	>1.89	1.18	>1.33	>1.49	1.74	1.35	>1.63	>1.72	>2.86	1.31	>1.57	1.79	2.12
$\Delta a/L$	2.98	>4.98	>5.81	>6.50	2.84	>4.98	>5.81	3.04	2.75	>4.98	>5.81	>6.50	2.54	>4.98	>5.81	4.63

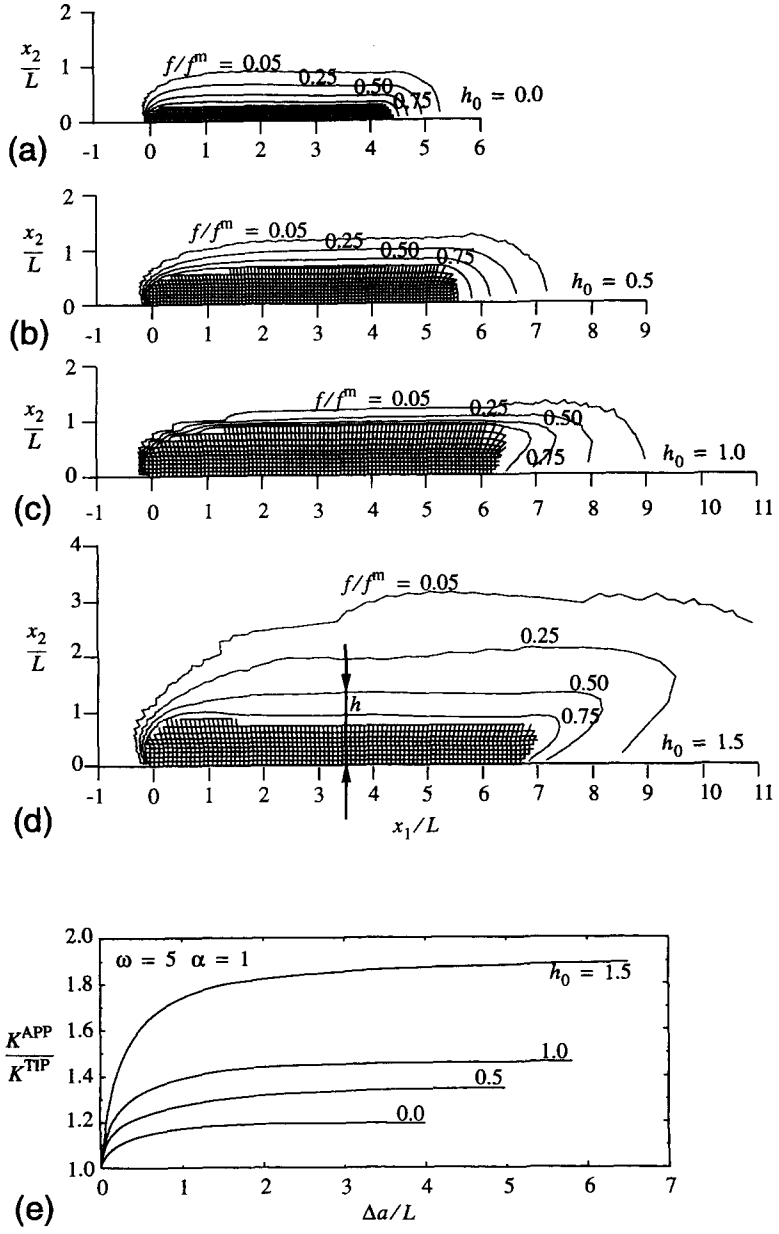

Fig. 7. Transformation zones (a)–(d) when $\Delta a = 4L$, $4.98L$, $5.81L$ and $6.50L$, respectively, and the crack growth resistance curve (e) for the case $\omega = 5$ and $\alpha = 1$ with various values of h_0.

from fully transformed to untransformed material remains smooth, indicating that the transformation behaviour does not approach the critical regime. In this case, increasing the value of h_0 results in transformation zones that are more diffuse and that have larger frontal zones. When the strength of the transformation is increased to $\omega = 10$, as shown in Figs 9 and 10, similar trends are observed. However, in general, the transformation behaviour appears to be less critical, which is probably caused by a larger redistribution of stresses due to the transformation.

Several experimental studies of the shape and the size of the transformation zone are available in the literature [see, for example, Marshall *et al.* (1990), Rühle and Evans (1989) and Yu and Shetty (1990)]. Depending on the material, these works indicate various kinds of transformation zone shapes. The front of the zone found by Marshall *et al.* (1990), seems to be similar to the rounded shape found for a purely dilatant material, while Rühle and Evans (1989), for ZTA materials, indicate a zone shape that has the same characteristics

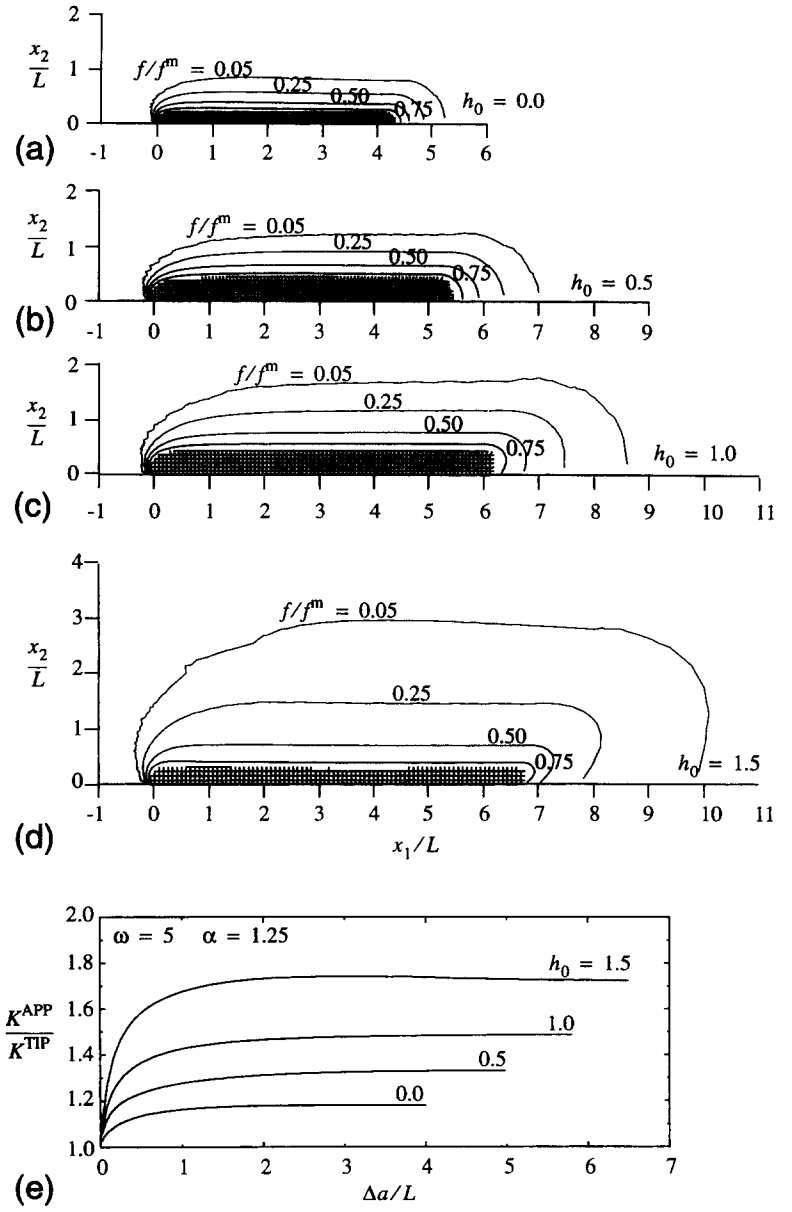

Fig. 8. Transformation zones (a)–(d) when $\Delta a = 4L$, $4.98L$, $5.81L$ and $6.50L$, respectively, and the crack growth resistance curve (e) for the case $\omega = 5$ and $\alpha = 1.25$ with various values of h_0.

as found here for sufficient large values of h_0. It is emphasized however that completely different experimental techniques for visualization of the transformation zone have been used in the above references, and that it is far from straightforward to directly relate those experimental observations to the transformation zones shown in Figs 6–10 in terms of transformed volume fraction. A thorough comparison of transformation zone shape as well as size needs more work and is outside the scope of the present paper.

As there is some experimental evidence of shear bands in PSZ and TZP materials (Chen and Reyes-Morel, 1986; Reyes-Morel and Chen, 1988), any information about the direction in which these bands are most likely to develop is of interest. It should be recalled that we have chosen our material parameters such as to *a priori* exclude the possibility of localization into a shear band, for example, with the constitutive model of Section 2. A study of shear band formation is outside the scope of the present paper. Nevertheless, it is of interest to have some insight in the directions into which the transformation shear is

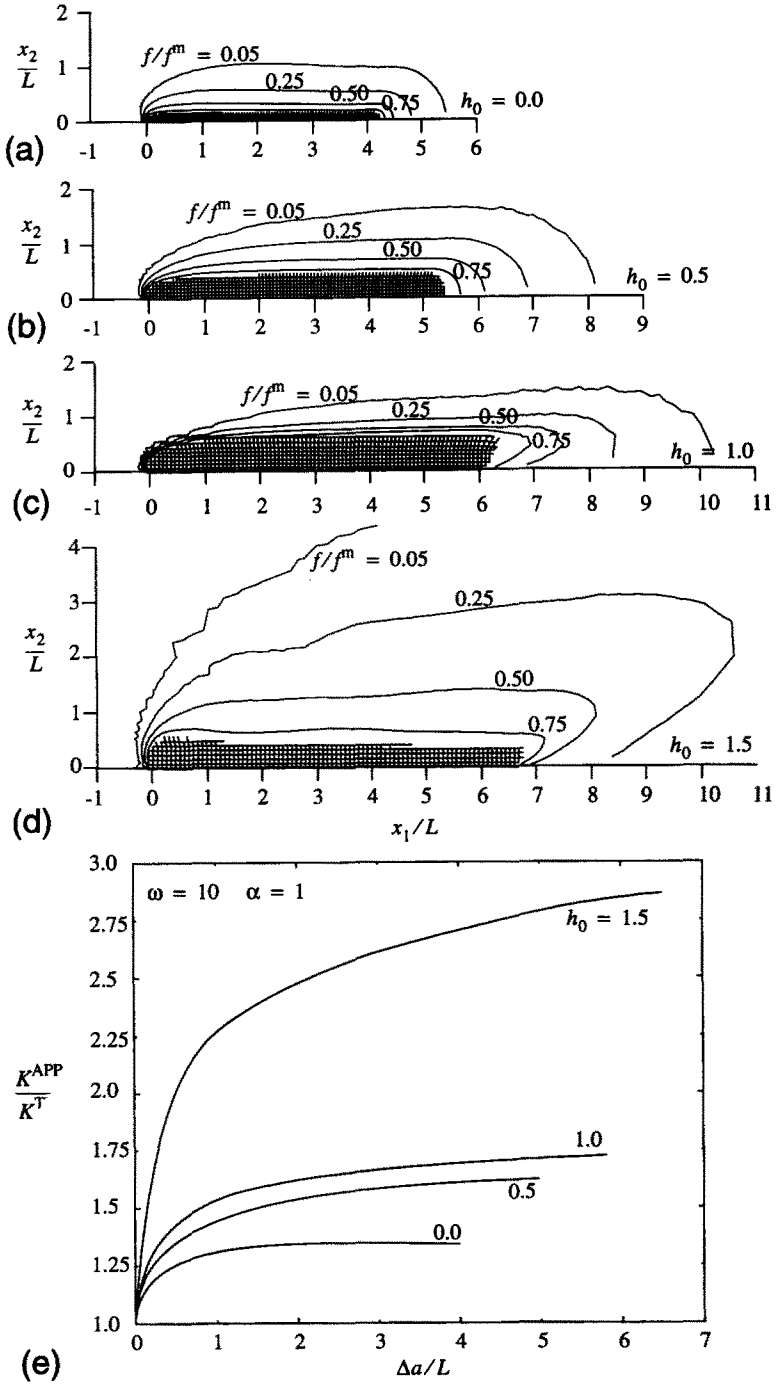

Fig. 9. Transformation zones (a)–(d) when $\Delta a = 4L$, $4.98L$, $5.18L$ and $6.50L$, respectively, and the crack growth resistance curve (e) for the case $\omega = 10$ and $\alpha = 1$ with various values of h_0.

most profound. Therefore, we have computed the directions of the "octahedral" planes at which the transformation shear strain reach maximum values. For the case $\omega = 10$ and $\alpha = 1.0$, the direction of the transformation shear strain is visualized in Fig. 11 by way of the orientation of crosses; the size of the crosses indicates the value of the maximum transformation shear strain. From this figure, there seems to be a tendency that increasing the value of h_0 causes a change in the shear directions close to the crack surface from $\pm 45°$ towards around $60°$ to $-30°$. Moreover for $h_0 = 1.5$ it is remarkable that initially the

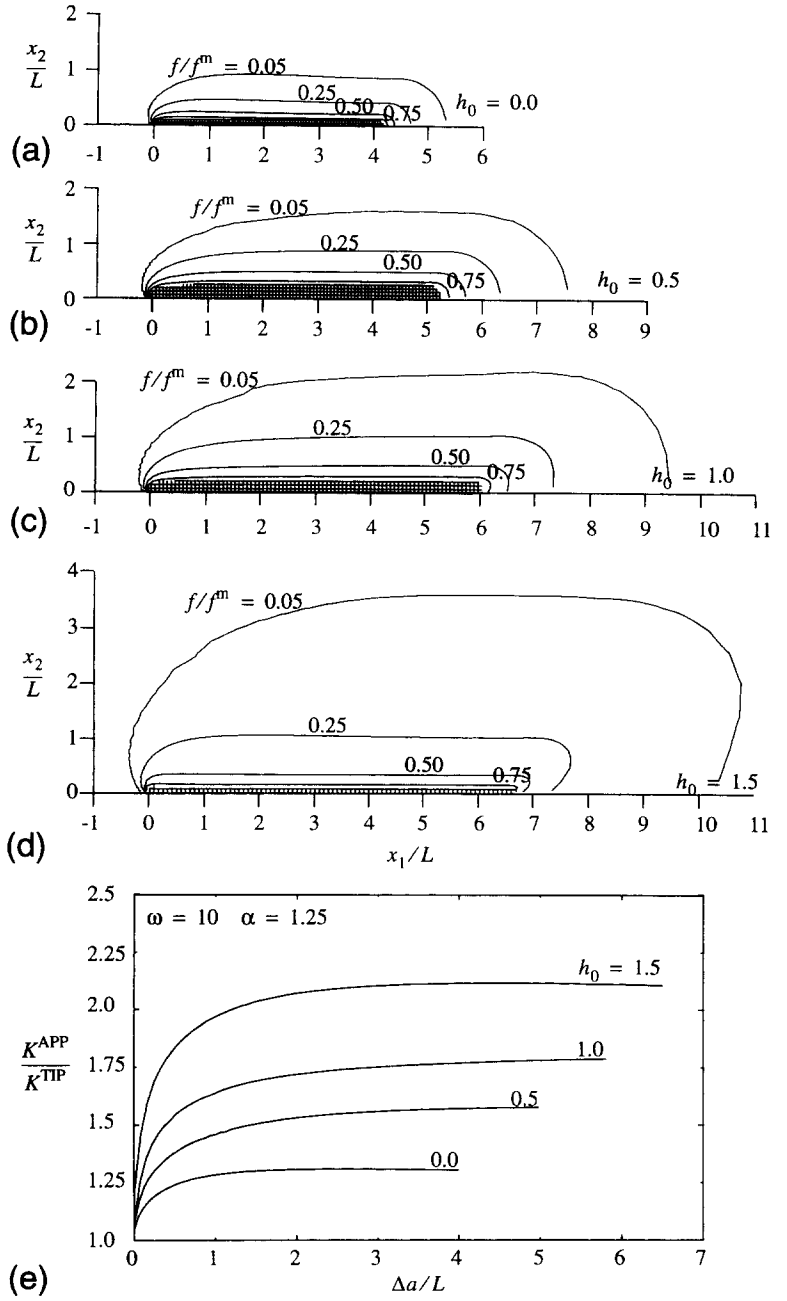

Fig. 10. Transformation zones (a)–(d) when $\Delta a = 4L$, $4.98L$, $5.81L$ and $6.50L$, respectively, and the crack growth resistance curve (e) for the case $\omega = 10$ and $\alpha = 1.25$ with various values of h_0.

transformation shear strains develop in a well-defined direction of $\sim 60°$ to $-30°$, while after some crack growth, the value of the maximum shear near the crack surface decreases. For $h_0 = 0.5$ and 1.0 the value of the maximum transformation shear strain remains more or less constant during crack advance. These analyses have been repeated with $\alpha = 1.25$ and/or $\omega = 5$, but these trends did not change significantly and the results will not be shown further.

As an illustrative example, the crack tip opening at various stages of crack growth is shown in Fig. 12 for the parameters $\omega = 10$, $\alpha = 1$ and $h_0 = 1.5$. For illustrative purposes, the crack opening displacements are reflected (scaled by a factor 12.3) to show the actual crack shape. In the first stage (I) shown in Fig. 12, no crack growth has yet occurred but

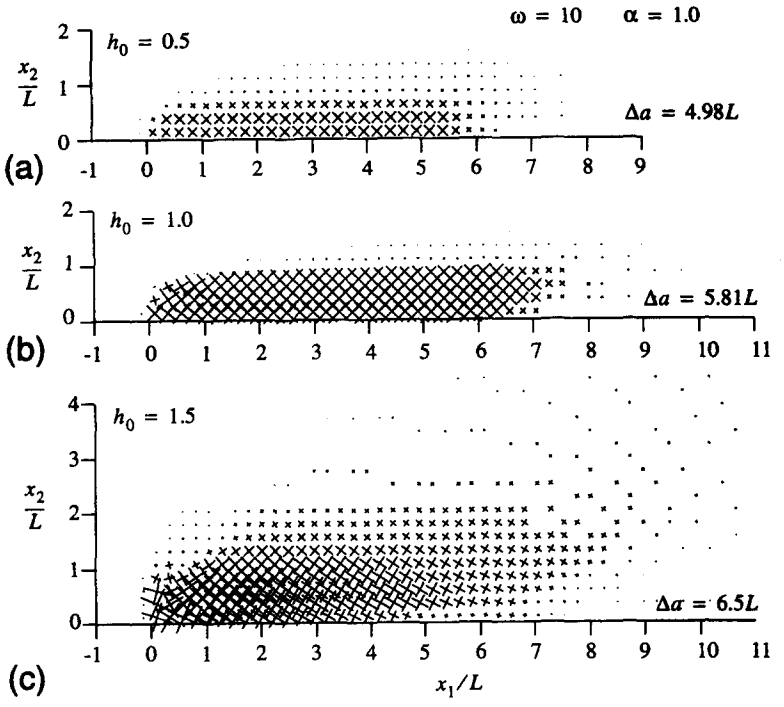

Fig. 11. Direction of the maximum transformation shear strains for the case $\omega = 10$ and $\alpha = 1$; (a) $h_0 = 0.5$, (b) $h_0 = 1$ and (c) $h_0 = 1.5$.

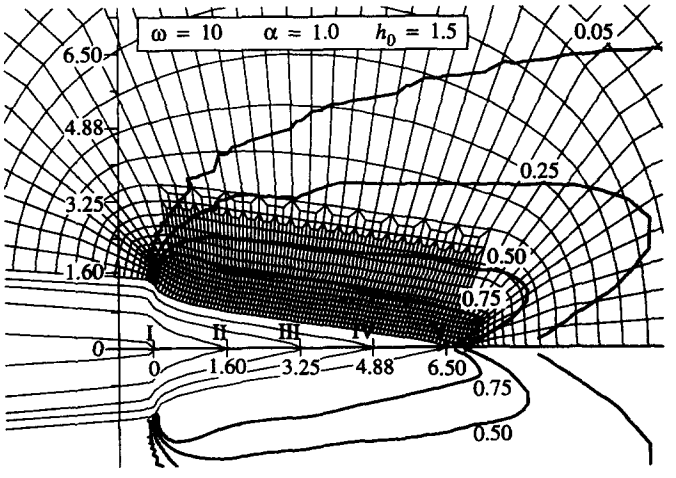

Fig. 12. Crack tip opening for various amounts of crack growth, $\Delta a = 0$, $1.6L$, $3.25L$, $4.88L$ and $6.50L$. At $\Delta a = 6.50L$ the deformed mesh is drawn and contours for f/f^m are shown. The deformations are scaled by a factor 12.3.

some crack tip blunting has occurred. It is seen that as the crack propagates, the crack faces are pushed towards another due to the phase transformation. In the final stage, V, shown in Fig. 12, the deformed mesh is also drawn, along with contours of f/f^m.

Toughness development

Prior to any crack growth it is found that for $h_0 = 0$ the initial toughness is not changed by the transformation strains, while for $h_0 > 0$ it seems that the initial toughness is increased. However, when the mesh is further refined a decreasing initial toughness value is found, which finally converges to a value of about 80% of the critical toughness of the material when the mesh is about ten times as fine. Thus prior to any crack growh, embrittling of the

material seems to takes place, but after the slightest crack extension the toughness increases drastically and picks up with the values shown in Figs 7–10. Similar convergence checks were performed after crack growth had occurred, and showed that the fineness of the mesh could be reduced to the currently used meshes to obtain converged results for crack growth analysis.

The toughness increase, expressed in terms of K^{APP}/K^{TIP}, as a function of crack advance $\Delta a/L$ for each of the cases mentioned above is shown in Figs 7(e)–10(e). As observed for purely dilatant materials already by Hom and McMeeking (1990), the crack growth resistance exhibits R-curve behaviour, i.e. the toughness generally tends to increase during the first stage of crack growth, then reaches a maximum, followed by a slight decrease before it settles down at the stationary value for steady-state growth. From these figures as well as from Table 1 we may note that, similar to the development of the transformation zone height, the maximum value for toughening has not yet been reached in some cases for which further crack growth would be necessary.

Evidently, the effect of transformation-induced shear strains on the crack growth resistance is of central importance. It is clearly seen from Figs 7(e)–10(e) that for all values of ω and α considered here, the toughness is increased significantly with increasing value of h_0. Even a relatively small contribution of transformation shear strains, represented by $h_0 = 0.5$, roughly doubles the toughness increase that is obtained when the transformation would be purely dilatant ($h_0 = 0$). Larger values of h_0 result in an even higher toughness increase, but the enhancement depends on the values of ω and α. There does not appear to be a clear relationship though between the value of h_0 and the crack advances at maximum crack growth resistance. Like in the purely dilatant case, the toughness increases with the strength of the transformation as characterized by ω. It can also be seen that the peak as well as steady-state values of the toughness generally increase with decreasing value of α, irrespective of h_0. The lower the hardening parameter α, the more material is fully transformed and the higher is the toughness increase.

7. CONCLUSION

In this paper, we have presented numerical studies of transient crack growth in ceramic composites exhibiting transformation-plasticity based on the recent model of Sun *et al.* (1991) that includes the effect of transformation-induced dilatation as well as shear. Our analyses supplement those of Hom and McMeeking (1990) who only considered dilatational transformations. The finite element results obtained here with the Sun *et al.* (1991) model show a very significant influence of the transformation shear strains on the transformation zone size and shape, as well as on the toughness development during crack growth. An increasing influence of the shear effect, as governed in the model by the parameter h_0, roughly speaking, leads to larger and more diffuse transformation zones. The increase of toughness with increasing value of h_0 has been found to be quite substantial as compared with the toughness increase that is obtained by purely dilatational transformation only. For values of h_0 between 1 and 1.5, which are representative for ZrO_2 composites, we have found improvements of toughness that are four to eight times larger than without transformation-induced shear strains. Since, so far, dilatant transformation-based theory has underestimated the toughness enhancement found in experiments (Evans and Cannon, 1986), the present results with transformation-induced shear effects contribute to explaining this difference. However, any definite conclusions to that effect will have to await a more detailed comparison with experiments on specific materials.

The predictions presented here have been obtained with values of the hardening parameter α that are representative of the experimental values suggested by Sun *et al.* (1991). Smaller values of α would probably have given even stronger toughening, with the limit being set by the occurrence of a supercritical response. We emphasize that for the values of α used in the present study, localization analysis has indicated that the behaviour will be subcritical for all deformation paths, and indeed in our crack growth computations we have not experienced any sign of loss of ellipticity.

It is pertinent here to relate the present work to the first analysis of transformation shear effects by Lambropoulos (1986). There are a number of differences with the constitutive model that he applied as well as his analysis of the small scale transformation problem. Regarding the constitutive model, we have to refer of course to the original paper of Sun *et al.* (1991) for details, but we mention two of the most important differences with the model of Sun *et al.* used here. First and foremost, Lambropoulos assumed that the $t \rightarrow m$ transformation occurs at the same moment for all transformable particles and proceeds to completion at once; this is similar to what Budiansky *et al.* (1983) called supercritical behaviour. As mentioned before, here we focused primarily on subcritical behaviour as this was suggested by experiments. We have found that with increasing contributions of transformation-induced shear strains, there is tendency to develop rather large and diffuse transformation zones; clearly, this does not support Lambropoulos' assumptions. Secondly, in Lambropoulos' model the particle is assumed to be incapable of supporting any shear load at transformation, whereas here the stresses inside transformed particles are related to the matrix stress state through an Eshelby type of argument, which is likely to give a more accurate representation. Finally, Lambropoulos assumes that the level of transformation within the transformation zone is small enough so that an asymptotic analysis can be used in which the stress state as the boundary of the transformation zone is approached from outside, is approximately the same as the unperturbed elastic solution. Here, full account is given of the effect of transformation-plasticity on the near-field stress fields. Supplementary to the present study, Stam and van der Giessen (1993) have studied crack growth in materials where the hardening parameter was chosen as $\alpha = 1$ corresponding to (at least near-) supercritical behaviour, and found that only for very low strengths of the transformation, say $\omega < 0.1$, an asymptotic analysis gives reasonable agreement with the numerical results.

In relating studies like the present one with real polycrystalline ceramic materials, it should be kept in mind that we have applied a continuum mechanics approach here. As put forward by Lambropoulos (1986) and others, the validity of the continuum approach may be questionable in some cases when the transformation zone height only spans a few grains. According to data given by Budiansky *et al.* (1983), the height of the transformation zone for a typical PSZ material is 0.6 μm. With a typical size of 0.3 μm for the transformable lens-shaped particles, it follows that the number of particles over the height is only about two. For a TZP material described by Reyes-Morel and Chen (1988), it was found that the height of the transformation zone varies between 0.1 and 1 mm. Thus, with a typical grain size of 2 μm it follows that the transformation zone spans many (50–500) particles, from which we may conclude that for the latter material the continuum approach may be valid. For PSZs, however, further detailed analysis of $t \rightarrow m$ transformations in individual particles would be necessary to quantify the minimum number of grains over the transformation height for which the continuum model is still valid. Also, we want to emphasize that the results presented here are only valid for small scale transformations, and the model predictions cannot be applied when the transformation zone is spread widely throughout the test specimen.

In the present work we have limited our parameter study to values of the strength ω of the transformation up to $\omega = 10$. However, experimental work on TZP materials by Reyes-Morel *et al.* (1988), for example, indicates values of ω that are twice as large. Results for larger values of ω will be published elsewhere. Further, we have excluded in our analyses the possibility of reverse transformations. However, some authors have reported reversible transformation (Marshall and James, 1986) and shape memory effects (Reyes-Morel *et al.*, 1988). The constitutive model used here is potentially capable of describing these phenomena, and as it is not unlikely that reversible transformation does occur in places where unloading takes place as a result of for instance crack growth, this requires further investigation. This work is currently in progress and will be published elsewhere.

REFERENCES

Budiansky, B., Hutchinson, J. W. and Lambropoulos, J. C. (1983). Continuum theory of dilatant transformation toughening in ceramics. *Int. J. Solids Structures* **19**, 337–355.

Budiansky, B. and Truskinovsky, L. (1993). On the mechanics of stress-induced phase transformation in zirconia. *J. Mech. Phys Solids* **41,** 1445–1459.

Chen, I. W. and Reyes-Morel, P. E. (1986). Implications of transformation plasticity in zirconia-containing ceramics: I, shear and dilatation effects. *J. Am. Ceram. Soc.* **69,** 181–189.

Chen, I. W. and Reyes-Morel, P. E. (1987). Transformation plasticity and transformation toughening in Mg-PSZ and Ce-TZP. *Mat. Res. Symp. Proc.* **78,** 75–88.

Eshelby, J. D. (1961). Elastic inclusions and inhomogeneities. In *Progress in Solid Mechanics II* (Edited by Sneddon, I. N. and Hill, R.), pp. 89–140. North-Holland, Amsterdam.

Evans, A. G. and Cannon, R. M. (1986). Toughening of brittle solids by martensitic transformations. *Acta Metall.* **34,** 761–800.

Evans, A. G. and Heuer, A. H. (1980). Review—transformation toughening in ceramics: martensitic transformations in crack-tip stress fields. *J. Am. Ceram. Soc.* **63,** 241–248.

Green, D. J., Hannink, R. H. J. and Swain, M. V. (1989). *Transformation Toughening of Ceramics*, CRC Press, Boca Raton, FL.

Hom, C. L. and McMeeking, R. M. (1990). Numerical results for transformation toughening in ceramics. *Int. J. Solids Structures* **26,** 1211–1223.

Hutchinson, J. W. (1974). On steady quasi-static crack growth. Harvard University Report TR74-1042.

Lambropoulos, J. C. (1986). Shear, shape and orientation effects in transformation toughening. *Int. J. Solids Structures* **22,** 1083–1106.

Marshall, D. B. and James, M. R. (1986). Reversible stress-induced martensitic transformation in ZrO_2. *J. Am. Ceram. Soc.* **69,** 215–217.

Marshall, D. B., Shaw, M. C., Dauskardt, R. H., Ritchie, R. O., Readey, M. J. and Heuer, A. H. (1990). Crack-tip transformation zones in toughened zirconia. *J. Am. Ceram. Soc.* **73,** 2659–2666.

McMeeking, R. M. and Evans, A. G. (1982). Mechanics of transformation-toughening in brittle materials. *J. Am. Ceram. Soc.* **65,** 242–246.

Mori, T. and Tanaka, K. (1973). Average stress in matrix and average elastic energy of materials with misfitting inclusions. *Acta Metall.* **21,** 571–574.

Ortiz, M., Leroy, Y. and Needleman, A. (1987). A finite element method for localized failure analysis. *Comp. Meth. Appl. Mech. Engng* **61,** 189–214.

Reyes-Morel, P. E. and Chen, I. W. (1988). Transformation plasticity of CeO_2-stabilized tetragonal polycrystals: I, stress assistance and autocatalysis. *J. Am. Ceram. Soc.* **71,** 343–353.

Reyes-Morel, P. E., Cherng, J. S. and Chen, I. W. (1988). Transformation plasticity of CeO_2-stabilized tetragonal zirconia polycrystals: II, pseudoelasticity and shape memory effect. *J. Am. Ceram. Soc.* **71,** 648–657.

Rice, J. R. (1968). Mathematical analysis in the mechanics of fracture. In *Fracture*, Part II (Edited by H. Liebowtiz), pp. 191–311. Academic Press, New York.

Rice, J. R. (1976). The localization of plastic deformation. In *Theoretical and Applied Mechanics* (Edited by W. T. Koiter), pp. 207–220. North Holland, Amsterdam.

Rühle, M. and Evans, A. G. (1989). High toughness ceramics and ceramic composites. *Progress in Mat. Sci.* **33,** 85–167.

Stam, G. Th. M. (1992). Analysis of crack growth in materials with transformation plasticity, theoretical background. TU Delft, Laboratory for Engineering Mechanics, LTM 978.

Stam, G. Th. M. and Van der Giessen, E. (1993). Analysis of supercritical transformation with dilatation and shear effects during crack growth in ceramics. In *Topics in Applied Mechanics* (Edited by J. F. Dijksman and F. T. M. Nieuwstadt), pp. 137–146. Kluwer, Dordrecht.

Stump, D. M. (1991). The role of shear stresses and shear strains in transformation toughening. *Phil. Mag.* **A64,** 879–902.

Sun, Q. P., Hwang, K. C. and Yu, S. U. (1991). A micromechanics constitutive model of transformation plasticity with shear and dilatation effect. *J. Mech. Phys. Solids* **39,** 507–524.

Turner, C. E. (1979). Methods for post-yield fracture safety assessment. In *Post-yield Fracture Mechanics* (Edited by Latzko), pp. 23–210. Applied Science, London.

Yu, C.-S. and Shetty, D. K. (1990). Transformation yielding, plasticity and crack-growth-resistance (*R*-curve) behaviour of CeO_2 TZP. *J. Mat. Sci.* **25,** 2025–2035.